Available online at www.sciencedirect.com
ScienceDirect
Journal of the European Ceramic Society 26 (2006) 3575–3582
www.elsevier.com/locate/jeurceramsoc

R-curve behaviour of 2Y-TZP with submicron grain size

Jens Eichler [a], Mark Hoffman [b], Ulrich Eisele [c], Jürgen Rödel [a,*]

[a] *Institute of Materials Science, University of Technology, Darmstadt, Petersenstr. 23, D-64287 Darmstadt, Germany*
[b] *The School of Materials Science and Engineering, University of New South Wales, Sydney, Australia*
[c] *Robert Bosch GmbH, FV/FLW, P.O. Box 106050, D-70049 Stuttgart, Germany*

Received 13 August 2005; received in revised form 22 November 2005; accepted 25 November 2005
Available online 10 January 2006

Abstract

Nanocrystalline powders were used to prepare fracture test specimens of 2Y-TZP with average grain sizes between 150 and 900 nm. Crack extension and attendant R-curve behaviour were studied in both air and vacuum. The plateau values in air and vacuum increase linearly with grain size from 3.1 to 5.1 MPa $m^{1/2}$ and from 4.7 to 6.7 MPa $m^{1/2}$, respectively. The size of the process zone was quantified using Raman microscopy and the results correlated to both the plateau values and the shape of the R-curve as a function of grain size.

Keywords: ZrO_2; Toughness and toughening; Fracture; Mechanical properties; Raman microscopy; R-curve

1. Introduction

The introduction of nanocrystalline powders for the processing of materials may potentially lead to a series of interesting phenomena. From a technological point of view, the enabled decrease in sintering temperature is very attractive, as it affords new combinations of materials for the cosintering of multilayers, especially the usage of metals with low melting temperatures. Furthermore, the use of nanocrystalline powders allows processing of materials with nanometer-sized grains which potentially also present exceptional properties, as, e.g. a better wear resistance.[1] Considerable efforts have recently lead to production of nanocrystalline powders on an industrial scale and a large push for related materials into the marketplace. Before these materials may be used, however, a better understanding of their mechanical properties is required.

Nanocrystalline Y-TZP is particularly attractive as it may allow cosintering with silver for use in oxygen sensors. Since only small specimens of this material were available to date, evaluation of mechanical properties has been limited to Vickers indentation studies.[2–4] It has been pointed out, however, that indentation methods provide artificially high values of toughness in transformation toughened ceramics.[5] Further complications arise due to severe plastic deformation below the indentation so that half penny shaped cracks do not form.[6] Furthermore, crack trapping from radial indentation cracks was reported in zirconia materials.[7] A study of nanocrystalline Y-TZP is further complicated by the fact that the retention of a fine grain size during sintering may be difficult.[8,9]

Transformation toughening[10] is known to be the dominant toughening mechanism in zirconia and leads to an extensive R-curve behaviour.[11,12] Currently, most reliable R-curve studies have been conducted for grain sizes greater than 500 nm. For this grain size regime the models for transformation toughening are established.[13,14] It is also widely known that the fracture toughness of Y-TZP materials increases with increasing grain size and decreasing dopant content within this grain size regime, although the exact dependencies are still a topic of debate.[15]

Wang et al.[16] observed a linear increase in fracture toughness with grain sizes of 0.8–2 μm for Y-TZP from 5 to 12 MPa $m^{1/2}$ measured by the Vickers indentation technique. Notably, after reaching a critical grain size the fracture toughness began to decrease again which was attributed to premature phase transformation and microcrack formation. The critical grain size was 0.87, 1.34 and 1.46 μm for yttria dopant concentrations of 2, 2.5 and 3Y-TZP, respectively. A smaller critical grain size of 250 nm for 2Y-TZP has also been reported.[2] Becher and Swain[15] reported a linear increase on a log–log plot in fracture toughness from 2.5 to 11 MPa $m^{1/2}$ for 2Y-TZP in the grain size regime from 0.5 to 1.5 μm using the double cantilever beam technique.

* Corresponding author. Tel.: +49 6151 166302; fax: +49 6151 166314.
E-mail address: roedel@ceramics.tu-darmstadt.de (J. Rödel).

0955-2219/$ – see front matter © 2005 Elsevier Ltd. All rights reserved.
doi:10.1016/j.jeurceramsoc.2005.11.012

R-curves are generally described by a constant crack-tip toughness K_0 and a shielding term K_μ, which is dependent on crack length. Stress-induced phase transformation occurs at a critical stress, σ_c. Assuming an unconstrained elastic stress field, stress declines with distance from the crack according to:

$$\sigma \propto \frac{K_{tip}}{\sqrt{r}} \tag{1}$$

where K_{tip} is the stress intensity factor at the crack tip. Phase transformation will, therefore, occur within a distance h from a crack defined by:

$$h \propto \left(\frac{K_{tip}}{\sigma_c}\right)^2 \tag{2}$$

The shielding term K_μ may then be realised as a linear function of K_{tip} as[13]:

$$K_\mu = \frac{\eta E \varepsilon_T V_f h^{1/2}}{1-\nu} = C_{AS} K_{tip} \tag{3}$$

with η a constant depending on process zone form and the stress field inside the transformation zone, E the Young's modulus, ν the Poisson's ratio, ε_T the dilatant strain accompanying phase transformation (4 vol.%), V_f the volume content of transformed particles and C_{AS} the shielding term which is independent of K_{tip}. The Poisson's ratio for Y-TZP is 0.33.[17] McMeeking and Evans[13] found η to be 0.21 by assuming that hydrostatic stress was responsible for phase transformation. Studies have verified the square root dependence of K_μ on the height of the transformation zone (e.g. Swain[18]), who also showed that the zone width as well as K_μ increased with grain size for Y-TZP. For subcritical transformation, η reduces linearly with the amount of non-transformed tetragonal phase.[19] The stress field declines with the distance from the crack tip as per Eq. (1) and a distribution of grain sizes leads to different transformation stresses for each individual grain. Subcritical transformation is therefore more probable for Y-TZP.[20] In a first approximation an intermediate amount of transformation can be assumed.[21]

Dopant concentration and grain size primarily affects the critical transformation stress for phase transformation and thereby the width of the process zone, h, in Eq. (2) and, hence, the shielding term and the rise of the R-curve up to the plateau.[13] Generally, two features of the phase transformation can be used to measure the zone width. Dilation causes: (a) an uplift of the surface, which may be detected by a measurement with atomic force microscopy[22,23] or Nomarski-Interference[24] or (b) displacements which may be measured using optical interferometry.[24] Alternatively, the monoclinic phase content within the transformation zone size may be measured by Raman microscopy down to a spatial resolution of ~1 μm.[18,25,26]

In a parallel study, the mechanical properties of submicron 3Y-TZP were studied.[27,28] The reduction in grain size from 500 nm down to 100 nm lead to a marked decrease in fracture toughness. To compensate, the dopant content was reduced to 2 mol% yttria (2Y-TZP), for this work. Here, the results for crack extension in air are shown for grain sizes of 150–500 nm and are compared to 3Y-TZP. As a rising R-curve could not be obtained with measurements in air, crack extension in the vacuum of a field emission scanning electron microscope (FESEM) was also quantified. These data are particularly pertinent as Y-TZP is known to be very susceptible to subcritical crack growth,[29–31] which leads to a velocity dependence of the R-curve[32] in air for materials toughened by process zone mechanisms. To rationalize the toughening mechanism, transformation zone profiles were obtained using Raman microscopy. Finally, plateau values for the R-curves were compared for different grain sizes and correlated to widths of the process zone.

2. Experimental procedure

2.1. Specimen preparation

A nanocrystalline powder doped with 2 mol% yttria and grain size of 7.3 nm was supplied by The Institute of New Materials (Saarbrücken, Germany). The phase content was predominantly tetragonal with a small amount of 1–2 vol.% monoclinic phase present. Plates for both compact tension (CT) specimens and bend bars for Raman investigation were prepared.

For crack propagation studies sheets of the green body were formed[33] with dimensions in the green state of 1.5 mm × 50 mm. Sintering was performed with a heating and cooling rate of 5 K/min with a hold period of 1 h at the maximum temperature, which was chosen to give a variation in grain size (see Table 1). A 500 g ceramic plate was placed on top of the specimen to prevent warpage during sintering.

Sintered plates were cut to compact tension specimens of 35 mm × 33.6 mm. They were then ground on both sides yielding specimen thicknesses of approximately 0.8 mm. One side of the specimen was polished to a 1 μm diamond paste finish. Two holes were drilled into the CT-specimens and a notch of 1 mm width cut. Limited powder availability restricted the number of specimen manufactured to 3 (150 nm), 1 (225 nm), 2 (300 nm) and 1 (500 nm) (grain sizes).

Bend bars for the Raman-microscopy studies were formed using uniaxial pressing of the powders in a die at 3 MPa and subsequent cold isostatic pressing at 510 MPa, but otherwise using the same heat treatment as before. After sintering they were ground on all four sides to approximate dimensions of 3 mm × 4 mm × 25 mm. One side was polished to a 1 μm diamond paste finish. At least four bend bars of grain sizes of 140, 280, 370, 490, 570 and 900 nm were prepared. All bend bars were utilized to determine the Young's modulus using the impulse excitation technique[34] with a resonance frequency and damping analyzer (RFDA-HT1750, IMCE, Diepenbeek, Belgium). Notches were introduced by a razor blade with diamond paste as an abrasive agent and the cracks formed by the bridge method, as in ASTM C 1421. No surface uplift could be observed near the crack using an AFM, therefore, subsequent analysis was undertaken with the samples using Raman microscopy.

2.2. Specimen characterization

X-ray diffraction studies (Model D500, Siemens, Karlsruhe, Germany) on the as-sintered specimens confirmed that the

specimens contained more than 97% tetragonal phase for the CT-specimens except for the 500 nm specimen, where 5% monoclinic phase has been found. The phase content was determined according to Toraya and Yoshimura[35] by comparing the area of the 1 1 1 reflex of the tetragonal phase with the combined area of the 1 1 1 and $-\underline{1}$ 1 1 reflex of the monoclinic phase. The density, ρ, was measured using the Archimedes method[36] for three specimens from each sintering batch. The relative density, ρ_{rel}, was calculated using a theoretical density of $\rho_t = 6.08\ g/cm^3$ for the tetragonal phase zirconia.[37]

Grain size was determined from measurements on fracture surfaces. Micrographs were taken with a FESEM (XL30 FEG, Philips, Eindhoven, Netherlands) and evaluated using the linear intercept method[38] via custom designed software.[39] A correction factor[33] of 1.48 was used to relate the two-dimensional grain size measurements to the three-dimensional grain size. At least 3 micrographs and a total of 300 intercepts were utilized for each sintering batch.

2.3. Crack extension studies

A custom designed mechanical testing device was used for crack propagation in CT-specimens.[40,41] Load was applied under displacement control by a piezoelectric actuator (PI Ceramic) and load measured using a 200 N load cell (FMD 200 N, Wazau, Germany) with an accuracy of ±0.2 N. Crack initiation was achieved using an indentation and a half chevron notch.[40,41] Renotching after crack initiation left a crack of length of about 100 μm. A heat treatment at 900 °C for 30 min reduced residual surfaces stresses which slightly decreased the measured fracture toughness by comparing the stress intensity factor for crack extension before and after the heat treatment. Retransformation of the initial transformation zone was not successful even at higher temperatures but lead to extensive thermal etching and the possibility of crack healing.

Crack extension with this same device was monitored both under ambient air environmental conditions with an optical microscope and in vacuum in the SEM. Crack length and applied load were recorded in both cases and the applied stress intensity factor, K_a, equivalent to the crack growth resistance K_R, calculated using ASTM E399.[42]

Crack extension in air was monitored by slowly increasing the load until crack extension was observed. The maximum load was recorded and then the load decreased to stop the crack propagation and the process repeated for another measurement. Data were taken at crack extension increments of approximately 20 μm to a total crack extension of at least 300 μm.

Crack extension measurements inside an evacuated FESEM (XL30 FEG, Philips, Eindhoven, Netherlands) chamber eliminate the influence of the environment upon fracture behaviour. Cable connections to the outside of the chamber enabled load control and data acquisition. Crack extension was monitored on the screen of the FESEM with a magnification of 7500×. A thin carbon layer was deposited on the CT-specimens to prevent charging of the surface. The carbon layer also allows accurate monitoring of the crack-tip position since it is transparent to the electron beam. Load was increased slowly until a sudden crack extension of 2–30 μm occurred. After this first jump crack propagation was stopped by decreasing the load instantaneously, maximum load and crack length recorded and the process repeated. A total crack extension of at least 300 μm was made. Care has to be taken with potential drifts of the load cell when used in vacuum. In our case a slight drift of 2–3 N (2–5% of maximum load) was observed and accounted for in the computation of $K_{R,vacuum}$ using ASTM E399.[42] Due to the complexity of the measurement, the number of specimens tested was limited to one specimen per grain size except for the 150 nm grain-size material where two specimens could be tested.

2.4. Raman microscopy

A confocal Raman microscope (Renishaw, New Mills, United Kingdom) was used to investigate the width of the transformation zone and the degree of phase transformation. The tetragonal and monoclinic zirconia phases have distinctly different Raman spectra[43,44] that can be recorded with up to 1 μm lateral resolution.[45] An Argon ion laser with a wave length of 514 nm was used with a 150 cm^{-1} cut-off filter. The spectral resolution was 1.7 cm^{-1} using a grid monochromator. The intensity was integrated over two minutes to minimize the background signal. The general equation to calculate the monoclinic phase content[45] could not be used since the tetragonal band at 148 cm^{-1} was cut off. Therefore a calibration was made using powders of greater than 98% monoclinic and 98% tetragonal phase content, respectively. The areas underneath the bands for the monoclinic phase $I_{m,100}$ (181 and 192 cm^{-1}) and tetragonal phase $I_{t,100}$ (264 cm^{-1}) were determined and the calibration factor κ for this apparatus was found to be 0.35. Fig. 1 shows a typical spectrum of a mixed specimen of monoclinic (grey) and tetragonal (black) phase with the chosen areas for the determination of the monoclinic phase

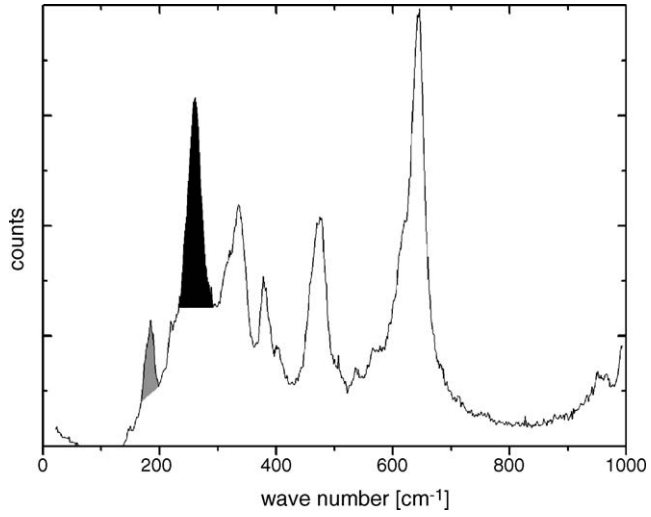

Fig. 1. Raman spectrum for a mixed monoclinic (grey) and tetragonal (black) specimen. The highlightedareas were used for the determination of the monoclinic phase content.

Table 1
Specimen characteristics for CT-specimens

Sintering temperature/holding time (°C/1 h)	Grain size (nm)	Density ρ (g/cm^3)	Relative density ρ_{rel} (g/cm^3)	Monoclinic phase content after sintering X (vol.%)
1110	150 ± 15	5.90 ± 0.03	97.0	0
1205	225 ± 25	5.91 ± 0.03	97.2	0
1275	300 ± 30	5.92 ± 0.01	97.4	<1
1405	500 ± 50	5.70 ± 0.05	93.8	5

content x_R:

$$x_R = \left(\frac{I_m^{181+192}}{I_m^{181+192} + \kappa I_t^{264}} \right) \quad \text{with} \quad \kappa = \frac{I_{m,100}}{I_{t,100}} \tag{4}$$

A spatial resolution across the crack of better than 2.5 μm was achieved by moving the microscope stage with the aid of micrometer screws.

3. Results

3.1. Specimen characterization

Tables 1 and 2 present the results of the specimen characterization for the CT-specimens and the bend bars, respectively. The minimum sintering temperature was chosen such that a density of at least 97% was reached. Then the peak temperatures were adjusted to attain grain sizes of 150, 225, 300 and 500 nm for the CT-specimens. For the bend bars the grain size range was extended up to 900 nm. Fig. 2 shows two micrographs of fracture surfaces with grain sizes of 150 nm (Fig. 2a) and 500 nm (Fig. 2b), respectively. The density initially increased with maximum sintering temperature up to 1300 °C, and then slowly decreased. Above 1500 °C the maximum achievable density was reduced significantly.

The reduction in density with increasing sintering temperature was reflected in an equivalent reduction in Young's modulus, E (Table 2). For the specimens sintered at 1300 °C (370 nm grain size) a maximum value of $E = 210$ GPa is reached. For a sintering temperature of 1600 °C (900 nm grain size) this decreased to a value of 196 GPa. It can also be seen that the fraction of both intrinsic and transformed (Table 2) monoclinic phase on the fracture surface increased with grain size.

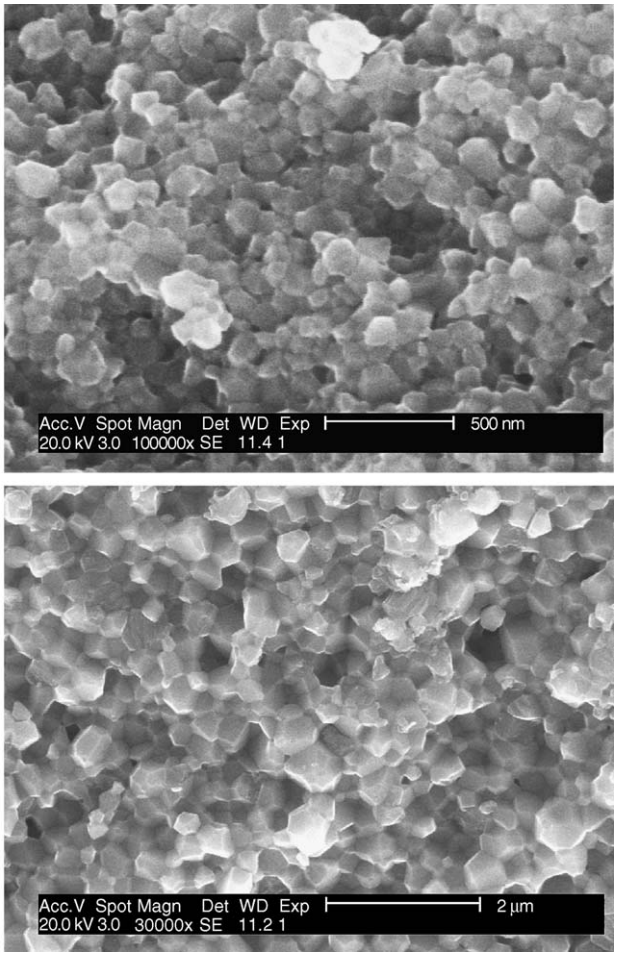

Fig. 2. SEM micrographs for 150 nm (a) and 500 nm (b) grain-size 2Y-TZP.

Table 2
Raman microscopy results and specimen characteristics of bend bars

Yttria content (mol%)	Grain size (nm)	Density (g/cm^3)	Monoclinic phase after sintering (vol.%)	Young's modulus (GPa)	Raman microscopy	
					Maximum monoclinic phase (vol.%)	Zone width (μm)
3	480	5.55 ± 0.08	<2	182 ± 3	9	1–2
2	140	5.87 ± 0.05	0	202 ± 1	11	2
2	280	5.99 ± 0.05	0	202 ± 3	23	2.5
2	370	6.00 ± 0.05	1	210 ± 3	24	2.5
2	490	5.97 ± 0.05	2.5	210 ± 1	27	3
2	570	5.96 ± 0.05	3	209 ± 2	30	3
2	900	5.83 ± 0.05	3	196 ± 1	38	4

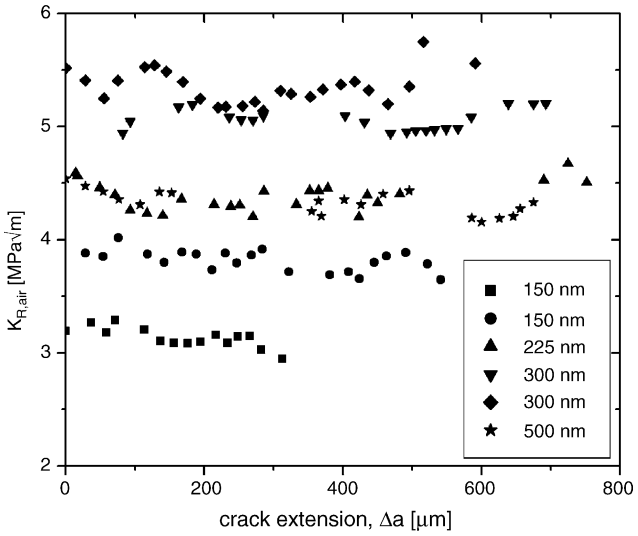

Fig. 3. Crack growth resistance, K_R, vs. crack extension, Δa, in air for 2Y-TZP for various grain sizes.

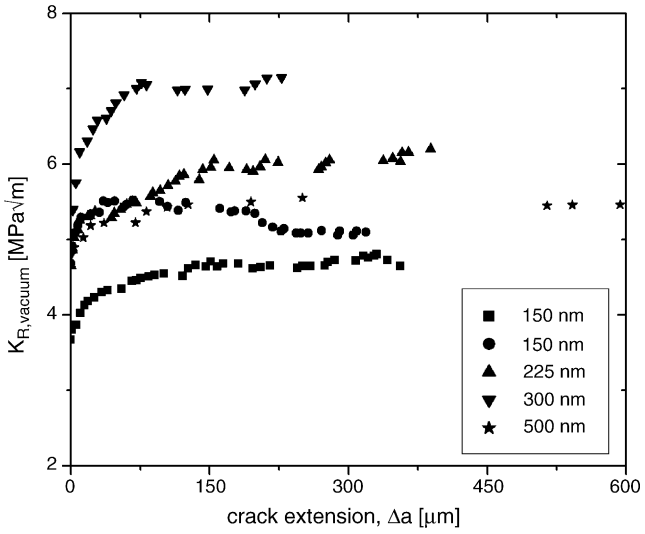

Fig. 4. Crack growth resistance, K_R, vs. crack extension, Δa, in vacuum for 2Y-TZP for various grain sizes.

3.2. Crack extension studies

Fig. 3 displays the results for crack extension in air for all specimens tested except specimen 1 in Table 3, as it is very similar to specimen 2. Grain size had a distinct effect on the fracture resistance, which did not change with crack extension in any case.

The absence of subcritical crack growth means that crack extension in vacuum is more erratic than in air and difficult to control. A slow increase in load leads to a controllable crack extension in increments of 1–5 μm. In between, the crack arrests for a short time and was stopped by decreasing the load. In some cases the crack had to overcome a localized higher resistance for crack extension. In order to further extend the crack a higher load was necessary which lead to a bigger crack extension of up to 30 μm. This may be prompted by local inhomogeneities in the material.

In Fig. 4 all recorded R-curves in vacuum are displayed. In all cases, an increase in fracture toughness is observed over the first 50–100 μm before a plateau is reached. Compared to the measurements in air, the plateau value is increased by 30–40%. There is a strong increase in toughness with crack extension and the plateau values increase for grain sizes up to 300 nm and then decrease for the 500 nm grain-size material. The second specimen with 150 nm grain size exhibited a sudden decrease in K_R that was not seen in any other specimen investigated. This is attributed to inhomogeneities in the specimen or a subsurface macroscopic flaw.

The 'plateau' toughness values shown in Table 3 for specimens tested in air were obtained by taking the average over all data points (in Fig. 3). The scatter within one data set is approximately 0.1 MPa $m^{1/2}$. The reproducibility of the results was shown by testing multiple specimens for some grain-size batches. The scatter between specimens is considerably higher than the scatter for each individual specimen. The plateau values of the R-curve increased from 3.1 MPa $m^{1/2}$ for a grain size of 150 nm up to 5.4 MPa $m^{1/2}$ for a grain size of 300 nm. For the 500 nm grain-size specimen the plateau value dropped to 4.3 MPa $m^{1/2}$ (Fig. 5).

For the specimens tested in vacuum the mean plateau toughness shown in Table 3 was obtained for all data points after

Table 3
Mechanical properties of 3Y-TZP

Grain size (nm)	Plateau value in air $K_{R,pl,air}$ (MPa $m^{1/2}$)	Plateau value in vacuum $K_{R,pl,vac}$ (MPa $m^{1/2}$)
150	3.1 ± 0.1	–
150	3.2 ± 0.1	4.7 ± 0.1
150	3.8 ± 0.1	5.3 ± 0.2
225	4.4 ± 0.1	5.9 ± 0.1
300	5.1 ± 0.1	6.7 ± 0.3
300	5.4 ± 0.2	–
500	4.3 ± 0.1	5.5 ± 0.1

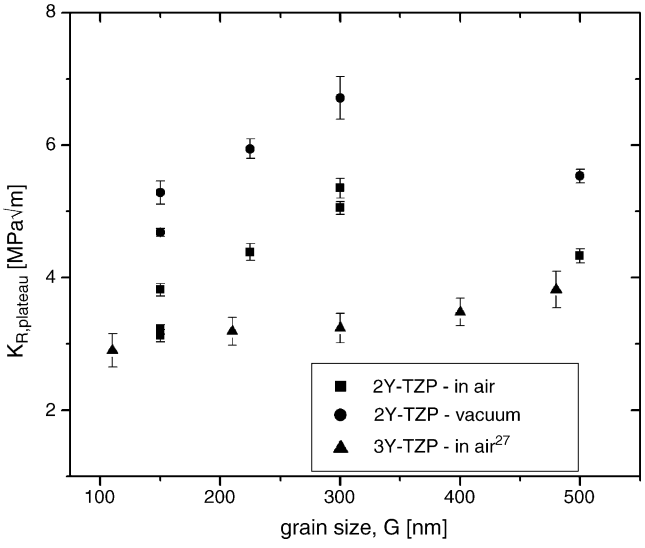

Fig. 5. Comparison of plateau toughness values, K_R, in vacuum and air for 2Y-TZP and in air for 3Y-TZP[27] as a function of grain size, G.

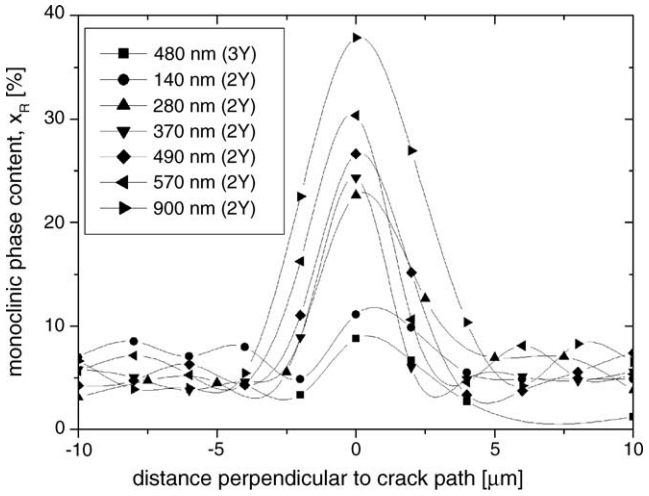

Fig. 6. Monoclinic phase content as a function of distance from the crack flanks in a bend bar for various grain-size 2Y-TZP materials. One 3Y-TZP material with 480 nm grain size is shown also for a compact tension sample.

reaching the R-curve plateau (in Fig. 4). The scatter within each value was between 0.1 and 0.3 MPa $m^{1/2}$. Fig. 5 shows that the mean plateau toughness values increased linearly with grain size in both vacuum and in air for grain sizes of 150–300 nm. Plateau toughness fell again for the 500 nm grain-size specimen, however, it should be noted that this specimen had exceptionally high porosity.

3.3. Raman microscopy

In Fig. 6 the monoclinic phase content as a function of distance from the crack flanks is shown as compared to a CT-specimen of 3Y-TZP with 480 nm grain size.

The maximum amount of transformation and the zone size (width at half the maximum height) for the different specimens is presented in Table 2. For the 3Y-TZP specimen with a grain size of 480 nm, the monoclinic phase content was 9% and the zone width between 1 and 2 μm. Due to the decrease in dopant concentration, larger zone sizes were attained for 2Y-TZP. For the 140 nm grain-size material, the maximum transformed amount was 11% and the zone size 2 μm. With increasing grain size, the maximum amount of transformation and the zone size increased up to 38% monoclinic phase and 4 μm zone size for the material with a grain size of 900 nm.

4. Discussion

4.1. Specimen characterization

Successful specimen preparation with grain sizes ranging from 150 to 500 nm was achieved for 2Y-TZP nanocrystalline powders to produce large specimens suitable for fracture mechanical evaluation. Densities higher than 97% were reached, except for the 500 nm grain-size specimen in the case of the CT-specimens. The microstructures appeared homogeneous (Fig. 2) and the crack extension studies pointed to few inhomogeneities. Grain growth was faster in 2Y-TZP than it was in 3Y-TZP.[27] Although the starting powder in the current work was much finer than for 3Y-TZP,[27] the final grain sizes at comparable temperatures (Table 1) were higher for 2Y-TZP. It appears, therefore, that the decrease in dopant concentration facilitates grain growth.

4.2. R-curve measurements and process zones

Crack propagation in air and vacuum in compact tension specimens was achieved for grain sizes ranging from 150 to 500 nm. The R-curve measurements in air show plateau values exhibiting a linear dependence with grain size. A comparison with the results of Wang et al.[16] shows that the data found here is approximately an extrapolation of the data gained for higher grain sizes. In contrast, Becher and Swain[15] found a linear relationship in a log–log plot for 0.5 to 11 μm. Contrary to Becher and Swain[15] and in agreement with Wang et al.[16] a critical grain size between 300 and 500 nm was found above which the fracture toughness decreases. Newer data by Bravo-Leon et al.[2] report a critical grain size of 250 nm. Therefore, 2Y-TZP for industrial applications is recommended to be used with grain sizes of less than 300 nm. For this grain-size regime plateau values of the R-curve of up to 5.4 MPa $m^{1/2}$ can be expected in an ambient air environment and up to 6.7 MPa $m^{1/2}$ in vacuum. A recent study by Gupta et al.[46] found a fracture toughness measured by the indentation method of 5.7 MPa $m^{1/2}$ for a grain size of 250 nm, which is comparable to the results in this study.

Comparing the plateau values of a parallel study on 3Y-TZP[27] in Fig. 4 with 2Y-TZP highlights a strong influence of yttria content on fracture toughness. With increasing grain size the reduction in dopant content becomes more critical and the increase in fracture toughness is more prevalent. At lower grain sizes the stabilization due to the low grain size is more dominant than the stabilization by the dopant. Bravo-Leon et al.[2] found fracture toughnesses as high as 16 MPa $m^{1/2}$ for grain sizes of around 100 nm for 1 and 1.5Y-TZP. Dopant concentrations of less than 2 mol% might therefore be difficult to control since small changes in grain size can lead to premature phase transformation and possibly microcracking.

The increase of fracture energy with crack extension could not be observed in air. The Raman-microscopy studies revealed that the height of the transformation zone for all 2Y-TZP materials is less than 3 μm. According to the model by McMeeking and Evans[13] 90% of the plateau of the fracture energy is reached at five times the height of the transformation zone. As initial crack lengths of less than 15 μm were not experimentally achievable, the rising part of the R-curve could not be recorded in air. In addition, the reverse transformation of the monoclinic phase to the tetragonal phase through annealing could not be achieved for the grain sizes considered here. Similar difficulties have been previously reported. For example, Fargas et al.[47] observed only a small increase in fracture toughness from 3.9 to 4.3 MPa $m^{1/2}$ in less than 50 μm for a grain size of 300 nm in 3Y-TZP.

The marked susceptibility of Y-TZP to subcritical crack growth is well documented.[30] With transformation toughening, the stress intensity factor at the crack tip K_{tip} (or its increase in going from air to vacuum) during crack propagation is directly

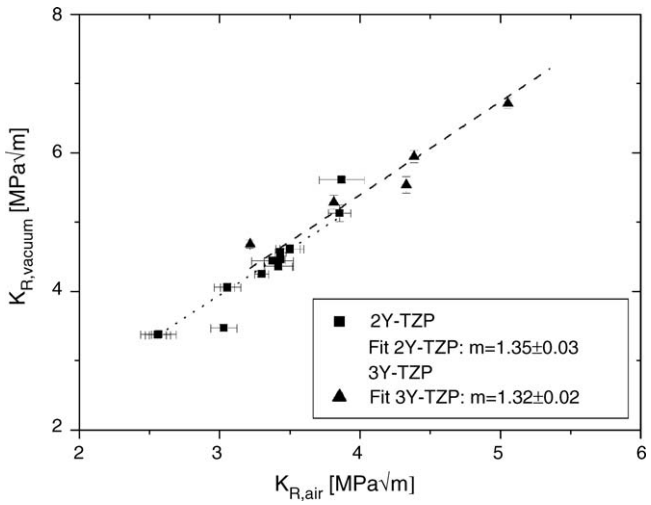

Fig. 7. Comparison of plateau toughness values in vacuum, $K_{R,vacuum}$, and in air, $K_{R,air}$, for 2Y-TZP and 3Y-TZP.[28] Linear regression curve goes through origin.

proportional to the shielding term K_μ via Eq. (3). Therefore:

$$\frac{K_{R,vacuum}}{K_{R,air}} = \frac{K_{tip,vacuum}}{K_{tip,air}} = \frac{K_{\mu,vacuum}}{K_{\mu,air}} \quad (5)$$

The usefulness of Eq. (5) is verified in Fig. 7 using results from this work for 2Y-TZP and the results for 3Y-TZP from a parallel study.[28] As the ratios of plateau values for vacuum and air are similar for 2Y-TZP and 3Y-TZP, it appears that their susceptibility to subcritical crack growth is also very similar.

Assuming that an undetected R-curve forms in air, crack propagation in vacuum will then produce rising crack resistance with the starting point of the R-curve consistent with the plateau value in air and the increase in fracture toughness limited to the increase in stress intensity factor at the crack tip ($K_{tip,vacuum} - K_{tip,air}$) and the accompanying shielding term ($K_{\mu,vacuum} - K_{\mu,air}$). Indeed, the starting values of the R-curves in vacuum in Fig. 4 are consistent with plateau values in air as displayed in Fig. 3.

The R-curves in Fig. 4 rise over a crack increment of 30–60 μm. According to McMeeking and Evans,[13] the width of the process zone is therefore in the order of 6–12 μm. As the plateau toughness value in vacuum is 30–40% higher than in air, application of Eq. (2) dictates that the process zone in vacuum should be about 70–100% wider as compared to that in air. This would predict a process zone in air of 3–8 μm, which is consistent with the results displayed in Fig. 6. This variation of process zone width and subsequent shielding, K_μ with the critical crack-tip stress intensity factor for crack propagation, K_{tip}, has also been reported in the case of cyclic fatigue-induced subcritical crack growth.[48]

5. Conclusions

Fracture test specimens of 2Y-TZP suitable were produced in the grain size regime of 150 to 500 nm. Crack growth resistance, in both air and vacuum, and phase transformability were measured and it was found that:

1. The extent of intrinsic monoclinic phase and also stress-induced tetragonal to monoclinic phase transformation at the crack flanks increased with grain size.
2. Consistent with this, the R-curve plateau toughness increased linearly with grain size, with the exception of the largest grain-size sample.
3. Plateau fracture toughness in vacuum was 30–40% higher than that observed in air.
4. This is a result of a reduced critical crack-tip stress intensity factor for crack propagation due to subcritical crack growth which subsequently results in a more sharply rising R-curve in air.

Acknowledgments

This work was supported by the Robert Bosch GmbH, Stuttgart, Germany, the Australian Research Council and the German Academic Exchange Service. Dr. Robert Moon is thanked for assistance with the Raman microscopy.

References

1. Basu, B., Lee, J.-H. and Kim, D.-Y., Development of nanocrystalline wear-resistant Y-TZP ceramics. *J. Am. Ceram. Soc.*, 2004, **87**(9), 1771–1774.
2. Bravo-Leon, A., Morikawa, Y., Kawahara, M. and Mayo, M. J., Fracture toughness of nanocrystalline tetragonal zirconia with low yttria content. *Acta Mater.*, 2002, **50**, 4555–4562.
3. Cottom, B. A. and Mayo, M. J., Fracture toughness of nanocrystalline ZrO_2–3 mol% Y_2O_3 determined by Vickers indentation. *Scripta Mater.*, 1996, **34**(5), 809–814.
4. Vasylkiv, O., Sakka, Y. and Skorokhod, V. V., Low-Temperature processing and mechanical properties of zirconia and zirconia–alumina nanoceramics. *J. Am. Ceram. Soc.*, 2003, **86**(2), 299–304.
5. Paterson, A. W. and Stevens, R., Comparison of indentation and notched bar toughness of TZP ceramics: relevance to models of the fracture process. *Int. J. High Technol. Ceram.*, 1986, **2**, 221–229.
6. Alcala, J. and Anglada, M., Indentation precracking of Y-TZP: implications to R-curves and strength. *Mater. Sci. Eng.*, 1998, **A245**, 267–276.
7. Cook, R. F., Braun, L. M. and Cannon, W. R., Trapped cracks at indentations: I. Experiments on yttria-tetragonal zirconia polycrystals. *J. Mater. Sci.*, 1994, **29**(8), 2133–2142.
8. Douglas, C. H. and Mayo, M. J., Sintering-forging of nanocrystalline zirconia: I. Experimental. *J. Am. Ceram. Soc.*, 1997, **80**(1), 149–156.
9. Srdic, V. V., Winterer, M. and Hahn, H., Sintering behavior of nanocrystalline zirconia prepared by chemical vapor synthesis. *J. Am. Ceram. Soc.*, 2000, **83**(4), 729–736.
10. Garvie, R. C., Hannink, R. H. and Pascoe, R. T., Ceramic steel? *Nature*, 1975, **258**, 703–704.
11. Casellas, D., Alcala, J., Llanes, L. and Anglada, M., Fracture variability and R-curve behavior in yttria-stabilized zirconia ceramics. *J. Mater. Sci.*, 2001, **36**, 3011–3025.
12. Sorensen, B. F., Brethe, P. and Skov-Hansen, P., Controlled crack growth in ceramics: the DCB specimen loaded with pure moments. *J. Eur. Ceram. Soc.*, 1996, **16**, 1021–1025.
13. McMeeking, R. M. and Evans, A. G., Mechanics of transformation-toughening in brittle materials. *J. Am. Ceram. Soc.*, 1981, **65**(5), 242–246.
14. Chen, I-W., Model of transformation toughening in brittle materials. *J. Am. Ceram. Soc.*, 1991, **74**(10), 2564–2572.
15. Becher, P. F. and Swain, M. V., Grain-size-dependent transformation behavior in polycrystalline tetragonal zirconia. *J. Am. Ceram. Soc.*, 1992, **75**(3), 493–502.

16. Wang, J., Rainforth, M. and Stevens, R., The grain size dependence of the mechanical properties in TZP ceramics. *Br. Ceram. Trans. J.*, 1989, **88**(1), 1–6.
17. Selcuk, A. and Atkinson, A., Elastic properties of ceramic oxides used in solid oxide fuel cells (SOFC). *J. Eur. Ceram. Soc.*, 1997, **17**, 1523–1532.
18. Swain, M. V., Grain-size dependence of toughness and transformability of 2 mol% Y-TZP ceramics. *J. Mater. Sci. Lett.*, 1986, **5**, 1159–1162.
19. Hannink, R. H. J., Kelly, P. M. and Muddle, B. C., Transformation toughening in zirconia-containing ceramics. *J. Am. Ceram. Soc.*, 2000, **83**(3), 461–487.
20. Evans, A. G., Perspective on the development of high-toughness ceramics. *J. Am. Ceram. Soc.*, 1990, **73**(2), 187–206.
21. Hsueh, C.-H., Becher, P. F. and Paul, F., Some considerations of nonideal transformation-zone profile. *J. Am. Ceram. Soc.*, 1988, **71**(6), 494–497.
22. Chen, X. Y., Zheng, X. H., Fang, H. S., Shi, H. Z., Wang, X. F. and Chen, H. M., The study of martensitic transformation and nanoscale surface relief in zirconia. *J. Mater. Sci. Lett.*, 2002, **21**, 415–418.
23. Meschke, F., Raddatz, O., Kolleck, A. and Schneider, G. A., R-curve behavior and crack-closure stresses in barium titanate and (Mg,Y)-PSZ ceramics. *J. Am. Ceram. Soc.*, 2000, **83**(2), 353–361.
24. Marshall, D. B., Shaw, M. C., Dauskardt, R. H., Ritchie, R. O., Readey, M. J. and Heuer, A. H., Crack-tip transformation zones in toughened zirconia. *J. Am. Ceram. Soc.*, 1990, **73**(9), 2659–2666.
25. Clarke, D. R. and Adar, F., Measurement of the crystallographically transformed zone produced by fracture in ceramics containing tetragonal zirconia. *J. Am. Ceram. Soc.*, 1982, **65**(6), 284–288.
26. Hoffman, M., Mai, Y. W., Dauskardt, R. H., Ager, J. and Ritchie, R. O., Grain size effects on cyclic fatigue and crack-growth resistance behaviour of partially stabilized zirconia. *J. Mater. Sci.*, 1995, **30**, 3291–3299.
27. Eichler, J., Eisele, U. and Rödel, J., Effect of grain size on mechanical properties of submicron 3Y-TZP: I. Subcritical crack growth and R-curve behavior. *J. Am. Ceram. Soc*, submitted for publication.
28. Eichler, J., Hoffman, M., Fett, T., Eisele, U. and Rödel, J., Effect of grain size on mechanical properties of submicron 3Y-TZP: II. Crack tip toughness and toughening effect. *J. Am. Ceram. Soc*, submitted for publication.
29. Chevalier, J., Olagnon, C. and Fantozzi, G., Subcritical crack propagation in 3Y-TZP ceramics: static and cyclic fatigue. *J. Am. Ceram. Soc.*, 1999, **82**(11), 3129–3138.
30. Knechtel, M., Garcia, D. E., Rödel, J. and Claussen, N., Subcritical crack growth in Y-TZP and alumina toughened Y-TZP. *J. Am. Ceram. Soc.*, 1993, **76**(10), 2681–2684.
31. Yin, H., Gao, M. and Wei, R. P., Phase transformation and sustained load crack growth in $ZrO_2 + 3$ mol% Y_2O_3: experiments and kinetic modelling. *Acta Metall. Mater.*, 1995, **43**(1), 371–382.
32. dos Santos e Lucato, S. L., Crack-growth-velocity-dependent R-curve behavior in lead zirconate titanate. *J. Am. Ceram. Soc.*, 2003, **86**, 1037–1039.
33. Kanters, J., *Sinterverhalten von Verbunden aus nanokristallinem Zirkoniumdioxid*, Ph.D. Thesis, Technical University Darmstadt, Germany, 2000.
34. Standard Test Method for Dynamic Young's Modulus, Shear Modulus, and Poisson's Ratio by Impulse Excitation of Vibration, E1876-00, 1099–1113, *Annual Book of ASTM Standards*, 3.01. The American Society of Testing and Materials, West Conshocken, 2001.
35. Toraya, H. and Yoshimura, M., Calibration curve for quantitative analysis of monoclinic-tetragonal ZrO_2 system by X-ray-diffraction. *J. Am. Ceram. Soc.*, 1984, **67**(6), 119–121.
36. Standard Test Methods for Apparent Porosity, Water Absorption, Apparent Specific Gravity, and Bulk Density of Burned Refractory Brick and Shapes by Boiling Water, C20-00, 6–8, *Annual Book of ASTM Standards*, 15.01. The American Society of Testing and Materials, West Conshocken, 2001.
37. Tsukuma, K., Kubota, Y. and Tsukidate, T., Thermal and mechanical properties of Y_2O_3-stabilized tetragonal zirconia polycrystals, 382, *science and technology of zirconia II*. In *Advances in Ceramics*, *Vol 12*, ed. N. Hrsg. Claussen, M. Rühle and A. H. Heuer. American Ceramic Society, OH, Westerville, 1984.
38. Standard Test Methods for Determining Average Grain Size, E112-96, 243-266, *Annual Book of ASTM Standards*, 3.01. The American Society of Testing and Materials, West Conshocken, 2001.
39. dos Santos e Lucato, S. L., *Lince v2.4-Linear Intercept*. Department of Materials Science, Technical University Darmstadt, Germany, 1999.
40. Rödel, J., Kelly, J. F. and Lawn, B. R., In situ measurements of bridged crack interfaces in the scanning electron microscope. *J. Am. Ceram. Soc.*, 1990, **73**(11), 3313–3318.
41. Rödel, J., Kelly, J. F., Stoudt, M. R. and Bennison, J., A loading device for fracture testing of compact tension specimen in the SEM. *Scanning Microsc.*, 1991, **5**(1), 29–35.
42. Standard Test Methods for Plane-Strain Fracture Toughness of Metallic Materials, E399–90, 408–438, *Annual Book of ASTM Standards*. The American Society of Testing and Materials, West Conshocken, 1997.
43. Keramidas, V. G. and White, W. B., Raman scattering study of the crystallization and phase transformations of ZrO_2. *J. Am. Ceram. Soc.*, 1974, **57**(1), 22–24.
44. Phillippi, C. M. and Mazdiyasni, K. S., Infrared and raman spectra of zirconia polymorphs. *J. Am. Ceram. Soc.*, 1971, **54**(5), 254–258.
45. Garvie, R. C. and Nicholson, P. S., Phase analysis in zirconia systems. *J. Am. Ceram. Soc.*, 1972, **55**(6), 303–305.
46. Gupta, N., Mallik, P. and Basu, B., Y-TZP ceramics with optimized toughness: new results. *J. Alloy.Compd.*, 2004, **379**, 228–232.
47. Fargas, G., Casellas, D., Llanes, L. and Anglada, M., Thermal shock resistance of yttria-stabilized zirconia with palmqvist indentation cracks. *J. Eur. Ceram. Soc.*, 2003, **23**, 107–114.
48. Hoffman, M. J., Wakayama, S., Mai, Y.-W., Kishi, T. and Kawahara, M., Crack-tip degradation processes observed during in situ cyclic fatigue of partially stabilised zirconia in the SEM. *J. Am. Ceram. Soc.*, 1995, **78**(10), 2801–2810.